Cerebral Cortex, June 2021;31: 2855–2867

doi: 10.1093/cercor/bhaa393
Advance Access Publication Date: 3 February 2021
Original Article

ORIGINAL ARTICLE

Metabolic and Hemodynamic Resting-State Connectivity of the Human Brain: A High-Temporal Resolution Simultaneous BOLD-fMRI and FDG-fPET Multimodality Study

Sharna D. Jamadar[1,2,3,†], Phillip G.D. Ward[1,2,3,†], Emma X. Liang[1], Edwina R. Orchard[1,2,3], Zhaolin Chen[1,4] and Gary F. Egan[1,2,3]

[1]Monash Biomedical Imaging, Melbourne, Vic, 3800 Australia, [2]Turner Institute for Brain and Mental Health, Monash University, Melbourne, Vic, 3800 Australia, [3]Australian Research Council Centre of Excellence for Integrative Brain Function, Melbourne 3800, Australia and [4]Department of Electrical and Computer Systems Engineering, Monash University, Melbourne, Vic, 3800 Australia

Address correspondence to Sharna D. Jamadar, 770 Blackburn Rd, Melbourne VIC 3800, Australia. Email: Sharna.jamadar@monash.edu.

[†]S.D.J. and P.G.D.W. have contributed equally to this work.

Abstract

Simultaneous [18F]-fluorodeoxyglucose positron emission tomography functional magnetic resonance imaging (FDG-PET/fMRI) provides the capacity to image 2 sources of energetic dynamics in the brain—glucose metabolism and the hemodynamic response. fMRI connectivity has been enormously useful for characterizing interactions between distributed brain networks in humans. Metabolic connectivity based on static FDG-PET has been proposed as a biomarker for neurological disease, but FDG-sPET cannot be used to estimate subject-level measures of "connectivity," only across-subject "covariance." Here, we applied high-temporal resolution constant infusion functional positron emission tomography (fPET) to measure subject-level metabolic connectivity simultaneously with fMRI connectivity. fPET metabolic connectivity was characterized by frontoparietal connectivity within and between hemispheres. fPET metabolic connectivity showed moderate similarity with fMRI primarily in superior cortex and frontoparietal regions. Significantly, fPET metabolic connectivity showed little similarity with FDG-sPET metabolic covariance, indicating that metabolic brain connectivity is a nonergodic process whereby individual brain connectivity cannot be inferred from group-level metabolic covariance. Our results highlight the complementary strengths of fPET and fMRI in measuring the intrinsic connectivity of the brain and open up the opportunity for novel fundamental studies of human brain connectivity as well as multimodality biomarkers of neurological diseases.

Key words: BOLD-fMRI, FDG-PET, fPET, functional connectivity, metabolic connectivity, resting-state, simultaneous MR-PET

Introduction

The invention of positron emission tomography (PET) in the 1970s (Ter-Pogossian 1992) and the development of functional magnetic resonance imaging (fMRI) in the early 1990s (Ogawa et al. 1990) have provided unique insights into brain function in living humans. During the past 2 decades, fMRI has been an enormously powerful tool for the discovery of intrinsic brain networks, the characterization of brain connectivity, and the identification of interactions between distributed brain networks (Fox et al. 2007; Fox and Raichle 2007). Recently, the advent of simultaneous [18F]-fluorodeoxyglucose PET (FDG-PET) and fMRI of the brain (Judenhofer et al. 2008) has provided the opportunity for unique new insights into the mechanisms of dynamic metabolic and neurovascular activity in the human brain (Villien et al. 2014).

Resting-state fMRI measures the temporal coherence of spontaneous neural activity between spatially distinct brain regions (Fox and Raichle 2007) and is normally measured using blood oxygenation level–dependent fMRI (BOLD-fMRI) (Biswal et al. 1995). Resting-state brain connectivity indexes spontaneous large-amplitude changes in blood oxygenation at low frequencies that have been associated with variability in cognition (Fox et al. 2007; Jamadar et al. 2016), individual differences in age (Andrews-Hanna et al. 2007), sex (Jamadar et al. 2018), and psychiatric and neurological conditions (Fornito and Bullmore 2010). Resting-state fMRI connectivity has potential as a biomarker of clinical progression for a number of neurological diseases, although its application as a diagnostic biomarker is currently limited (Hohenfeld et al. 2018).

BOLD-fMRI provides a hemodynamic-based surrogate index of neuronal activity with a temporal resolution in the order of seconds and submillimeter spatial resolution. The BOLD-fMRI signal is an indirect index of neuronal function, arising from neurovascular coupling between neuronal activity and cerebral hemodynamics (Phillips et al. 2016). While BOLD-fMRI is usually interpreted as arising from neuronal activity, there are a number of non-neuronal contributors to the BOLD signal, including heart rate variability, respiration, head movement, individual variability in hemoglobin, and the oxygen-carrying capacity of the blood, etc. (Liu 2017; Ward et al. 2019). As such, BOLD-fMRI is a semiquantitative nonabsolute index of neural activity, and BOLD-fMRI responses cannot be quantitatively compared across brain regions, subjects, or imaging sites, or within the same individual across time (Logothetis 2008). These characteristics are a major limiting factor in the development of BOLD-fMRI–based biomarkers, particularly when derived from fMRI functional connectivity metrics (Hohenfeld et al. 2018).

Resting-state connectivity measured using other neuroimaging techniques provide a unique perspective on information transfer in the brain. Here, we investigate brain connectivity derived from FDG-PET to measure covariation of glucose uptake throughout the human brain—an index of cerebral metabolism. FDG-PET provides a snapshot of cerebral glucose uptake, and connectivity analyses of FDG-PET have characterized the covariation in cerebral glucose uptake across subjects (Horwitz et al. 1984; Moeller et al. 1987). This measure of "metabolic" connectivity is an important complement to BOLD-fMRI functional connectivity, since FDG-PET represents a more direct and quantitative measure of neuronal function than BOLD-fMRI. While evidence suggests metabolic connectivity shows moderate-to-strong correlation with fMRI connectivity (Di and Biswal 2012; Passow et al. 2015; Di et al. 2017; Savio et al. 2017), due to technical limitations, the majority of FDG-PET studies have acquired static images of the brain with an effective temporal resolution of the scan duration—10 to 40 min. Since static FDG-PET (sPET) acquisitions provide a single cumulative measurement per subject, metabolic "connectivity" was estimated "across-subjects." As such, these results are more accurately characterized as metabolic "covariance," rather than "connectivity." Covariance measures are not dependent on the temporal correlation of glucose uptake and therefore provide patterns that do not necessarily arise from coupled activity between brain regions. Furthermore, it is known from fMRI that group-level covariance poorly predicts individual measures of seed-based functional connectivity (Roberts et al. 2016). Consequently, FDG-sPET images cannot be used to estimate metabolic connectivity within single subjects, greatly limiting their application as a disease biomarker (Veronese et al. 2019; cf., Yakushev et al. 2017).

Recent advances in radiotracer delivery, together with the improved PET signal detection sensitivity of dual-modality magnetic resonance (MR)-PET scanners, has made it possible to study the dynamics of FDG-PET glucose uptake with substantially improved temporal resolution. The method described as "functional" FDG-PET (FDG-fPET) have achieved a temporal resolution of 60 s (Villien et al. 2014; Hahn et al. 2016, 2017; Li et al. 2019; Jamadar et al. 2019b) or less (Rischka et al. 2018; Jamadar et al. 2019a; Hahn et al. 2020). These methodological advancements have opened up an unprecedented opportunity to examine the temporal coherence of glucose metabolic signals across subjects, in a similar manner to BOLD-fMRI.

The goal of the present study was to investigate FDG-fPET metabolic connectivity with high-temporal resolution. We used FDG-fPET data with temporal resolution of 16 s and simultaneously acquired BOLD-fMRI data with a temporal resolution of 2.45 s. Two major hypotheses were tested in the present study. Firstly, we hypothesized that FDG-sPET metabolic covariance would be moderately associated with fPET metabolic brain connectivity. Secondly, we predicted that resting-state metabolic brain connectivity would be strongly associated with resting-state BOLD-fMRI connectivity.

Materials and Methods

All methods were reviewed by the Monash University Human Research Ethics Committee, in accordance with the Australian National Statement on Ethical Conduct in Human Research (2007). Administration of ionizing radiation was approved by the Monash Health Principal Medical Physicist, in accordance with the Australian Radiation Protection and Nuclear Safety Agency Code of Practice (2005). For participants aged over 18 years, the annual radiation exposure limit of 5 mSv applies and the effective dose equivalent was 4.9 mSv. Detailed information on the constant infusion acquisition procedure is available in Jamadar et al. (2019b). Data are available on OpenNeuro (see Data Availability Statement), and a data descriptor is available in Jamadar et al. (2020).

Participants

Participants ($n = 27$) were aged 18–23 years (mean 19 years), 20 female, all right handed (Edinburgh Handedness Inventory). Participants had between 13 and 18 years of education (mean 14 years), normal or corrected-to-normal vision, and no personal history of diagnosed Axis-1 mental illness, diabetes, or cardiovascular illness. Participants were screened for claustrophobia,

non-MR compatible implants, clinical or research PET scan in the past 12 months, and women were screened for current or suspected pregnancy. Prior to the scan, participants were directed to consume a high-protein/low-sugar diet for 24 h, fast for 6 h, and drink 2–6 glasses of water. Blood sugar level was measured using an Accu-Check Performa (model NC, Mannheim, Germany); all participants had blood sugar levels <10 mmol/L (max in this sample 4.73 mmol/L).

Procedure

Prior to the scan, participants completed a brief cognitive battery (30 min, results not reported here). Participants were then cannulated in the vein in each forearm with a minimum size 22-gauge cannula, and a 10-mL baseline blood sample was taken at the time of cannulation. For all participants, the left cannula was used for FDG infusion, and the right cannula was used for blood sampling. Primed extension tubing was connected to the right cannula (for blood sampling) via a 3-way tap.

Participants underwent a 95-min simultaneous MR-PET scan in a Siemens (Erlangen) Biograph 3-Tesla molecular MR scanner (Fig. 1*a*). Participants were positioned supine in the scanner bore with head in a 16-channel radiofrequency head coil and were instructed to lie as still as possible with eyes open and think of nothing in particular. FDG (average dose 233 MBq) was infused over the course of the scan at a rate of 36 mL/h using a BodyGuard 323 MR-compatible infusion pump (Caesarea Medical Electronics, Caesarea, Israel). One participant received a lower dose (167 MBq) due to infusion pump error. Infusion onset was locked to the onset of the PET scan.

Plasma radioactivity levels were measured throughout the duration of the scan. At 10-min postinfusion onset, a 10 mL of blood sample was taken from the right forearm using a vacutainer; the time of the 5-mL mark was noted for subsequent decay correction. Subsequent blood samples were taken at 10-min intervals for a total of 10 samples for the duration of the scan. The cannula line was flushed with 10 mL of saline after every sample to minimize line clotting. Immediately following blood sampling, the sample was placed in a Heraeus Megafuge 16 centrifuge (ThermoFisher Scientific, Osterode, Germany) and spun at 2000 rpm for 5 min; 1000 µL plasma was pipetted, transferred to a counting tube, and placed in a well counter for 4 min. The count start time, total number of counts, and counts per minute were recorded for each sample. Figure 1*b* shows the interpolated plasma radioactivity concentration over time. The average radioactivity concentration constantly increases over time with the lowest relative slope at the end of the acquisition.

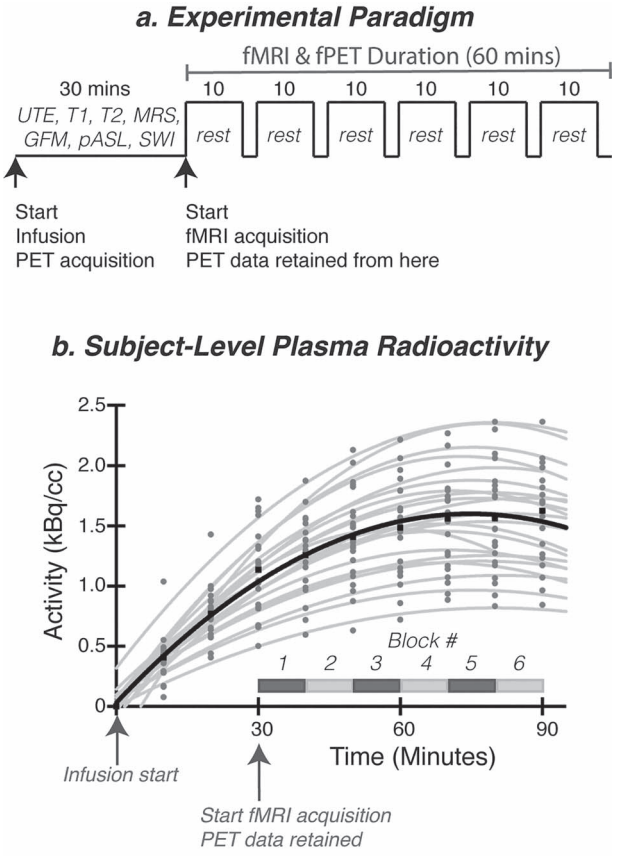

Figure 1. (*a*) Experimental paradigm. Participants underwent a 95-min simultaneous MRI-PET scan. FDG was infused over the course of the scan, with infusion start time locked to the onset of the PET scan (time 0). For the first 30-min, non-fMRI scans were acquired to allow the PET signal to increase to detectable levels (see Fig. 2, plasma radioactivity curve). At the 30-min timepoint, 6 consecutive 10-min resting-state BOLD-fMRI (T_2* echo planar imaging) blocks were completed. Participants rested quietly with eyes open with central fixation (cross) for the full 60 min. Abbreviations: GFM, gradient field map; pASL, pulsed arterial spin labelling; SWI, susceptibility weighted imaging. (*b*) Plasma radioactivity curve. Individual subject radioactivity curves are plotted in gray, with the average across all subjects plotted in black.

MR–PET Protocol

PET data were acquired in list mode. Infusion of FDG radiotracer and PET data acquisition started with the ultrashort time echo (UTE) MRI for PET attenuation correction (Fig. 1*a*). To allow the PET signal to rise to detectable levels, non-fMRI scans were acquired in the first 30 min following infusion onset. These scans, in order, were: ultrashort TE (UTE) (acquisition time, TA = 1.40 min), T_1 3D magnetization prepared rapid gradient echo (TA = 7.01 min, time repetition [TR] = 1640 ms, TE = 2.34 ms, flip angle = 8°, field of view (FOV) = 256 × 256mm^2, voxel size = 1 × 1 × 1 mm^3, 176 slices; sagittal acquisition), and several scans not reported here: T_2 sampling perfection with application optimized contrasts using different flip angle evolutions (SPACE) (TA = 5.52 min), MR spectroscopy (TA = 2.48 min), gradient field map (TA = 1.02 min), pulsed arterial spin labelling (TA = 4.21), T_2 susceptibility-weighted image (TA = 6.50 min), left–right phase correction (TA = 0.21 min). For the remainder of the scan, 6 consecutive 10-min blocks of T_2*-weighted echo planar images (EPIs) were acquired (TR = 2450 ms, TE = 30 ms, FOV = 190 mm, 3 × 3 × 3 mm^3 voxels, 44 slices, ascending axial acquisition).

MR Image Preparation

For the T_1 structural image, the brain was extracted, then registered to MNI152 space using advanced normalization tools (ANTs) (Avants et al. 2011). The gray matter, white matter, and brain cortex labels of T_1 image were segmented by using Freesurfer with Desikan-Killiany Atlas (Diedrichsen et al. 2009).

The 6 blocks of EPI scans for all subjects (a total of 245 EPIs) underwent a standard fMRI preprocessing pipeline. Specifically, all scans were brain extracted (FSL BET, Smith 2002), corrected for intensity nonuniformity using N4 bias field correction (ANTs, Tustison et al. 2010), motion corrected (FSL MCFLIRT, Jenkinson

et al. 2002), slice timing corrected (AFNI, Cox 1996), and high-pass filtered (Hz > 0.01) to remove low-frequency noise (FSL, Jenkinson et al. 2012). Across subjects, average mean framewise translational motion was 0.41 mm; maximum was 1.09 mm.

PET Image Reconstruction and Preparation

The 5700-s list-mode PET data for each subject were binned into 356 3D sinogram frames each of 16-s interval. The pseudoCT method (Burgos et al. 2014) was used to correct the attenuation for all acquired data. Ordinary Poisson-Ordered Subset Expectation Maximization algorithm (3 iterations, 21 subsets) with point spread function correction was used to reconstruct 3D volumes from the sinogram frames. The reconstructed DICOM slices were converted to NIFTI format with size $344 \times 344 \times 127$ (voxel size: $2.09 \times 2.09 \times 2.03$ mm ^{3}) for each volume. A 5-mm FWHM Gaussian postfilter was applied to each 3D volume. All 3D volumes were temporally concatenated to form a 4D ($344 \times 344 \times 127 \times 356$) NIFTI volume. A guided motion correction method using simultaneously acquired MRI was applied to correct the motion during the PET scan. We retained the 225 16-s volumes commencing from the 30 min timepoint, which matched the start of the BOLD-fMRI EPI acquisition, for further analyses. A single sPET image was derived from the sum of the 16-s volumes.

The 225 PET volumes were motion corrected (FSL MCFLIRT, Jenkinson et al. 2002); the mean PET image was brain extracted and used to mask the 4D data. The fPET data were further processed using a spatiotemporal gradient filter to estimate the short-term change in glucose uptake from the cumulative glucose uptake that was measured (Jamadar et al. 2020). The filter removed the accumulating effect of the radiotracer and other low-frequency components of the signal to isolate short-term resting-state fluctuations. This approach intrinsically adjusted for the mean signal while avoiding global-signal regression and other approaches that may create spurious anticorrelations in the data (Li et al. 2019; Murphy and Fox 2017). Due to radiotracer dynamics, it was not expected that the fPET sensitivity would be uniform across the 60 min of the resting-state data acquisition. As the radiotracer accumulated in the brain, it was anticipated that the signal-to-noise ratio (SNR) of the PET image reconstruction would progressively improve. The Supplement includes the definition of the spatiotemporal filter (Supplementary Fig. S1).

Connectivity Analyses

fPET and fMRI timeseries were extracted for each of the 82 regions of interest (ROIs) from the segmentation of the T_1-weighted image, interpolated using an ANTs rigid registration (Avants et al. 2011). To construct a connectivity matrix, Pearson's correlation coefficients were estimated between the timeseries from pairs of regions. This produced a single per-subject per-modality 82×82 matrix corresponding to the 60 min of resting-state in the experimental protocol. The 6 motion parameters were used to account for framewise displacement effects in the fPET and fMRI connectivity matrices. Thus, each region-by-region association is a partial correlation of region A, region B, pitch, roll, yaw, x, y, z for each subject, then averaged across subjects for the group connectome.

Group-Average Connectivity for BOLD-fMRI and FDG-fPET

The similarity between the group-average BOLD-fMRI and FDG-fPET matrices was assessed using a Pearson correlation across all edges on the lower triangle of the connectivity matrices (excluding the diagonal and symmetric triangle). The regional variation between the 2 modalities was assessed by calculating a separate correlation coefficient for each row of the connectivity matrix, providing a measure of similarity of the connectivity profile for each brain region.

sPET Metabolic Covariance

An FDG-sPET metabolic covariance matrix was constructed using the mean signal for each subject from the sPET image. The signal was de-meaned for each subject to remove intersubject variances, such as dosage and physiology. The across-subject correlation between pairs of ROIs was then estimated to generate the covariance matrix. The similarity of across-subject metabolic covariance of sPET and intersubject temporal correlation/metabolic connectivity of fPET was examined at a regional and global level. A comparison of the characteristics of the metabolic covariance and the metabolic connectivity was performed, assessing the scale of correlations and the network profile.

Spatial Maps of Region Degree

To further characterize and contrast connectivity from the 2 modalities, the strength of connections to each region were examined. Each connectivity matrix was discretised at the 90th percentile level to provide a binary graph of the "strongest" connections. We took this approach, rather than a threshold approach based on null hypothesis testing, as the SNR properties of each modality are substantially different. Thus, a common threshold across all 3 modalities would lead to many significant regions in some modalities (i.e., sPET) and very few in others (i.e., fPET). We argue that the percentile approach is appropriate in this analysis, as the goal was to examine and compare the distribution of most connected regions between modalities, without the additional concerns of subthreshold results. Results across other thresholds are reported in the Supplement. The number of these binary edges connected to each region was calculated to provide a map of regional degree for each modality.

Graph-Based Network Analysis

To investigate the patterns of connectivity within and between subnetworks, node degree was calculated and regions were sorted by subnetwork assignment (i.e., frontoparietal, dorsal attention, ventral attention, default mode, somatomotor, limbic, subcortical, and visual; as classified by Yeo et al. 2011. As the regions were not evenly distributed between subnetworks, some subnetworks (e.g., default mode network) contained a higher number of nodes than others. Therefore, there was a higher chance that significant edges would occur within subnetworks with more nodes by random chance. To minimize this bias in our interpretation, we adjusted node degree for the capacity of each network (number of observed edges, divided by number of potential edges between 2 subnetworks).

Shared Variance Between sPET & fPET and fMRI & fPET

To investigate the shared variance between the 2 modalities, the fPET connectome for each individual was regressed from the sPET and fMRI connectome, respectively. The standardized residuals of the regression were visualized in a matrix to show the distribution of variance not explained by fPET in the sPET and fMRI connectome.

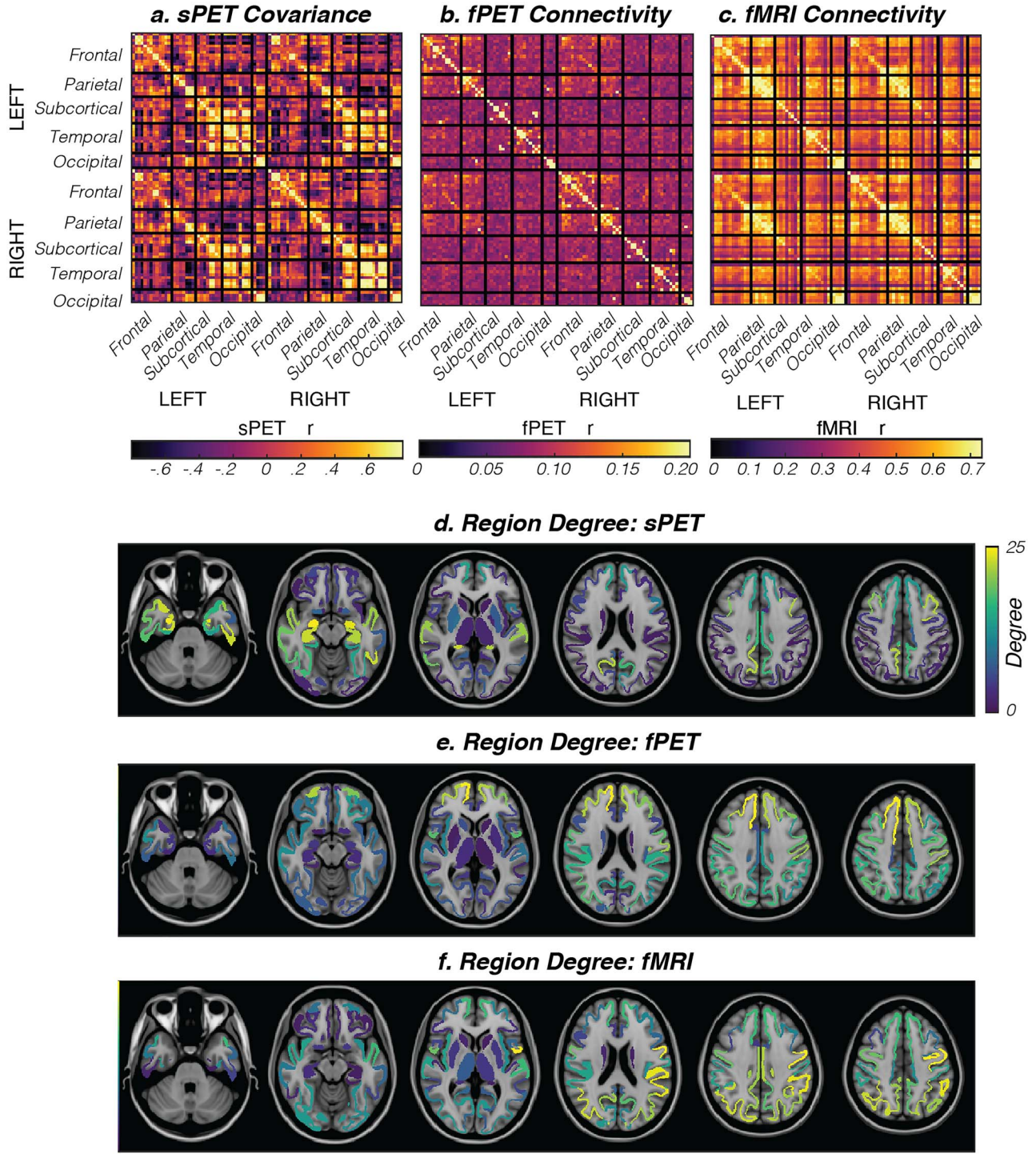

Figure 2. (*a*) FDG-sPET resting-state covariance matrix thresholded from $-0.65 < r < 0.65$. (*b*) FDG-fPET resting-state connectivity matrix thresholded from $0 < r < 0.12$. (*c*) BOLD-fMRI resting-state connectivity matrix thresholded from $0 < r < 0.75$. Supplementary Figure S1 shows the distribution of the number of edges across *r* values for each modality. (*d*) Spatial representation of the connection centrality (region degree; number of connections attached to the region) of FDG-sPET. (*e*) Spatial representation of the connection centrality (region degree) of FDG-fPET and (*f*) Spatial representation of the connection centrality (region degree) of BOLD-fMRI. Supplementary Figures S5–S7 show the variation of the region degree plots (panels *d*–*f*) across different thresholds.

Results

We first provide a qualitative overview of the sPET covariance, functional PET (fPET) connectivity, and fMRI connectivity matrices (Fig. 2), and their associated network graphs (Fig. 3). Secondly, we compare the sPET results to fPET, to determine if sPET covariance is predictive of fPET connectivity. Lastly, we compare fPET results with fMRI, to determine the relationship between metabolic and functional connectivity.

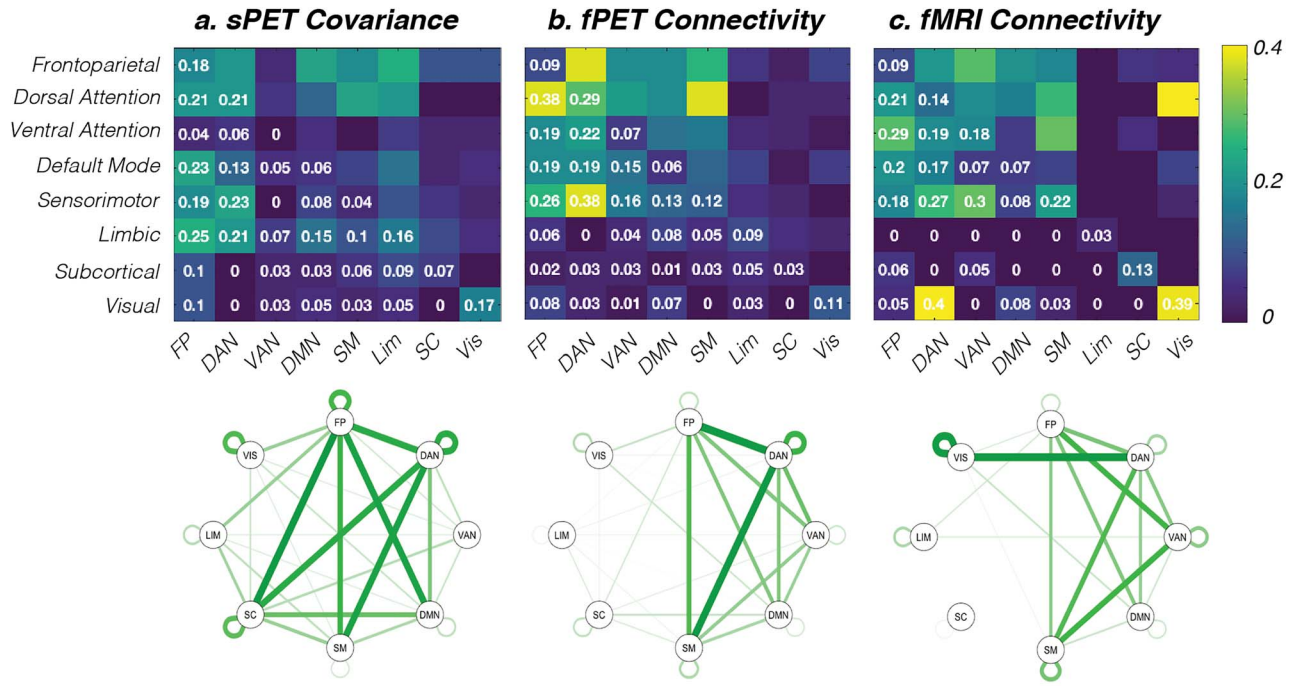

Figure 3. Connectivity matrices (top panel) and network graphs (bottom panel) for 8 canonical resting-state networks. Within-network connections lie on the diagonal (e.g., visual–visual) and between-network connections lie on the off-diagonal (e.g., visual-default mode). (*a*) FDG-sPET metabolic covariance, (*b*) FDG-fPET metabolic connectivity, and (*c*) BOLD-fMRI hemodynamic connectivity. Abbreviations: FP, frontoparietal network; DAN, dorsal attention network; VAN, ventral attention network; DMN, default mode network; SM, sensorimotor network; Lim, limbic network; SC, subcortical network; Vis, visual network.

Metabolic Covariance, Metabolic Connectivity, and Hemodynamic Connectivity

sPET Metabolic Covariance

The across-subject sPET metabolic covariance matrix showed large variability in connection strength across ROIs (Fig. 2*a*). Each cortical subdivision showed strong covariance with neighboring regions, as evident by the high-covariance values ($r \geq 0.5$; orange–yellow colors) along the main diagonal. Furthermore, each cortical subdivision showed strong homotopic covariance, as evident by the high covariance values along the diagonals of the top-right and bottom-left quadrants of the matrix. High temporosubcortical covariance was observed both within and between hemispheres; and high frontosubcortical, frontotemporal, and parieto-occipital covariance was also apparent, albeit of smaller magnitude than the temporosubcortical covariance. FDG-sPET showed the highest region degree in the temporal poles and subcortically (Fig. 2*d*). In the network graphs (Fig. 3*a*), sPET showed strong widespread connectivity between the dorsal attention, frontoparietal, subcortical, sensorimotor, and default mode networks.

fPET Metabolic Connectivity

The most salient effect for the group-averaged within-subject FDG-fPET metabolic connectivity matrix was the stronger ($r \geq 0.15$; orange–yellow colors) frontoparietal connectivity, both within and between hemispheres (Fig. 2*b*). Left–right homotopic connectivity was also evident for frontal and parietal cortices; this was not visually apparent for subcortical, temporal, and occipital cortices. fPET showed the highest degree in the frontal poles and the superior cortex (Fig. 2*e*). For the network graphs (Fig. 3*b*), fPET showed high connectivity between the frontoparietal and dorsal attention networks and between the dorsal attention and sensorimotor networks. Moderate connectivity was apparent between the sensorimotor–frontoparietal networks and between the default mode and dorsal attention, frontoparietal and visual attention networks. The dorsal attention network showed strong within-network connectivity as well.

fMRI Functional Connectivity

BOLD-fMRI showed strong ($r \geq 0.6$; orange–yellow colors) connectivity within anatomical subdivisions, both within and between hemispheres (Fig. 2*c*). This pattern was evident from the 4 diagonal lines in the fMRI connectivity matrix. A number of long-range connections between anatomical subdivisions were also evident, including frontoparietal, parieto-occipital, and temporoparietal regional connectivity. These long-range connections were evident both within and between hemispheres but were of smaller magnitude than the short-range and homotopic connections. Network graphs for the fMRI data (Fig. 3*c*) showed strongest connectivity between the dorsal attention and visual networks, with the visual network having the highest self-connectedness. The visual attention network showed high connectedness with the frontoparietal and sensorimotor network, and the default mode network showed an intermediate level of connectedness with the frontoparietal and dorsal attention networks. The anatomical projections of the most highly connected regions (Fig. 2*f*, lower row) indicated that the parietal cortex was most interconnected region in the fMRI data, with superior frontal and inferior occipital cortices showing intermediate levels of hemodynamic-based connectivity. Subcortical and orbitofrontal regions were the least interconnected regions in the BOLD-fMRI data.

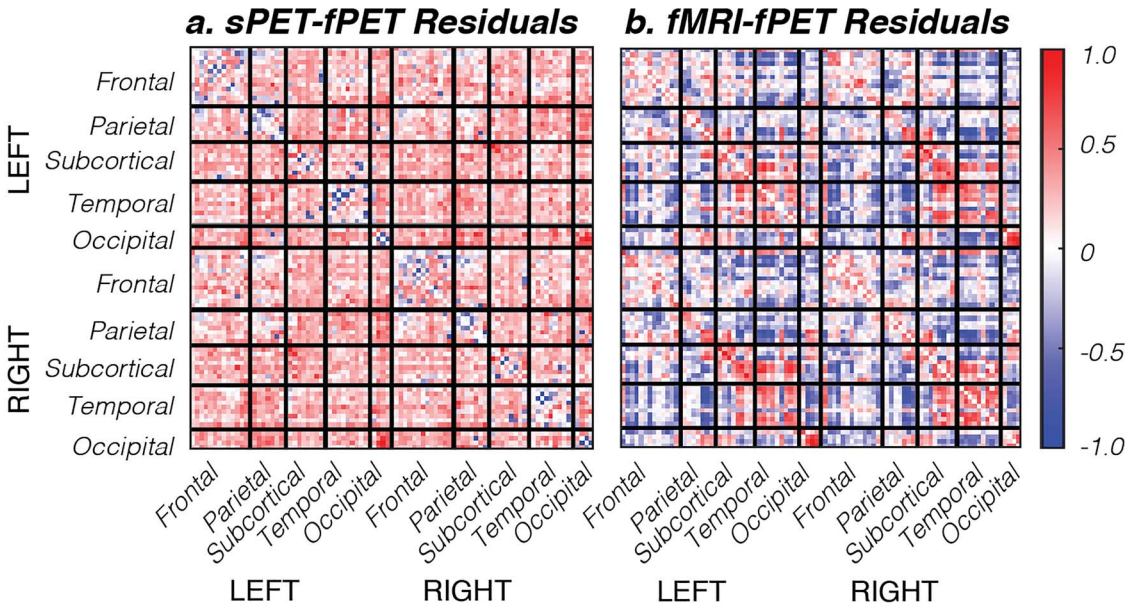

Figure 4. Matrix of residuals for the multiple regressions controlling for fPET variance for (*a*) sPET and (*b*) fMRI.

Comparison of FDG-sPET Metabolic Covariance and FDG-fPET Metabolic Connectivity

Qualitatively the sPET covariance and fPET connectivity matrices show little similarity (Fig. 2*a*,*b*). The fPET connectivity was dominated by frontoparietal connectivity, whereas the sPET covariance demonstrated greater variability throughout the connectivity matrix. The distribution of edges for each r value for sPET and fPET showed that fPET is biased toward positive r values, whereas sPET is symmetric around $r = 0$ (Supplementary Fig. S2). Comparison of the network graphs (Fig. 3) and the anatomical projections of the most connected regions (Fig. 2*d*–*f*) are consistent with the finding that sPET and fPET show little anatomical similarity across the brain. This result is confirmed by the matrix of sPET ~ fPET residuals (Fig. 4*a*), which highlights that sPET covariance has substantial variance ($e > 0.5$) that is unexplained by fPET connectivity. In particular, the left–right homologue covariance in the subcortical and temporal regions is not explained by fPET within-subject connectivity. Taken together, these results are consistent with the conclusion that across-subject sPET connectivity does not predict within-subject fPET connectivity. These results are not consistent with the hypothesis that static metabolic connectivity would be moderately associated with within-subject metabolic brain connectivity.

Comparison of FDG-fPET Metabolic Connectivity and BOLD-fMRI Hemodynamic Connectivity

Qualitatively the FDG-fPET metabolic connectivity and BOLD-fMRI hemodynamic connectivity matrices showed moderate similarity, with a trend toward stronger connectivity associated with the frontoparietal cortex (Fig. 2). Both fPET and fMRI network graphs (Fig. 3) showed strong connectivity for the dorsal attention network, with the dorsal attention network strongly connected to the frontoparietal network for fPET and strongly connected to the visual network for fMRI. The default mode network showed moderate connectedness for both fPET and fMRI. The matrix of the fMRI ~ fPET residuals (Fig. 4*b*) is relatively flat, with little variability across ROIs. Residual values were uniformly slightly positive ($e \sim 0.2$) suggesting a slight positive bias in variance for fMRI compared with fPET. Unlike the sPET ~ fPET residuals, there is little systematic variation across anatomical regions. These results are consistent with the conclusion that within-subject resting-state metabolic brain connectivity is more closely associated with resting-state hemodynamic connectivity than sPET metabolic covariance.

Discussion

In this study, we report for the first time resting-state metabolic brain connectivity measured using a novel FDG-fPET imaging protocol and methodology in humans. A key strength of this work is the simultaneous acquisition and high temporal resolution that enabled multimodality within-subject analyses of resting-state brain activity. The simultaneous acquisition of fPET and fMRI data is of particular importance, as measures of metabolic and hemodynamic responses to the same neural activity without the confound of intraindividual differences in attention, fatigue, motivation, nutrient intake, and blood chemistry that occur in sequential brain imaging experiments (Chen et al. 2018). We compared shared variance between within-subject fPET metabolic connectivity and across subject sPET metabolic covariance, and with BOLD-fMRI hemodynamic connectivity. Resting-state functional FDG-PET connectivity showed a high degree of unexplained variance between sPET covariance and fPET connectivity, and greater explained variance between fPET connectivity and BOLD-fMRI connectivity. Our study builds upon the foundations of earlier work that has used variants of PET to study the resting brain, including the seminal work of Fox, Raichle, Shulman, and colleagues who used O^{15} PET imaging of cerebral blood flow to delineate the default mode network (Shulman et al. 1997; Raichle et al. 2001) and Horwitz and colleagues (Horwitz et al. 1984; Azari et al.

1994) who conducted the first region-by-region correlation of neuroimaging signals using FDG-PET.

Metabolic Connectivity Is Predominantly Evident in Frontoparietal Regions

FDG-fPET metabolic connectivity was dominated by frontoparietal connectivity both within and between hemispheres. This is consistent with early evidence showing the frontoparietal cortices are highly metabolically active compared with temporo-occipital regions (Sasaki et al. 1986), particularly at rest (Shokri-Kojori et al. 2019; Vaishnavi et al. 2010). This pattern was confirmed by the brain network graphs where the dorsal attention network was strongly connected to the frontoparietal and sensorimotor networks and showed strong intraconnectedness. Together, the frontoparietal and dorsal attention networks are responsible for flexible, goal-directed behavior (Laird et al. 2011), and the two networks interact closely to subserve action-focused attentional control (Dixon et al. 2008). The interconnectedness of the frontoparietal and dorsal attention networks with the sensorimotor network is consistent with this interpretation. Interestingly, the dorsal attention and frontoparietal control networks have the highest metastability, update efficiency, and neural synchrony in comparison to other resting-state networks (Alderson et al. 2020). These networks demonstrate a resting-state configuration that is similar to a task-related configuration, which thereby facilitates dynamic and flexible switching between rest and task-active states. Our results support this interpretation and suggest that glucose metabolism in these networks is maintained at a high level in the resting-state, potentially to facilitate flexible switching to task-positive states when necessary.

The benefits of fPET methodology are two-fold. Firstly, FDG uptake is neurophysiologically closer to the process of interest—that is, neuronal function—than the BOLD response. It is well-known that BOLD-fMRI is an indirect index of neuronal activity that is not only ill-defined (e.g., Phillips et al. 2016), and nonquantitative (Logothetis 2008), but is also confounded by physiological parameters (e.g., Ward et al. 2019). In contrast, most of the glucose uptake measured by FDG-PET is localized to the synapses (Sokoloff et al. 1977; Sokoloff 1981; Magistretti and Allaman 2015). As noted by (Raichle and Snyder 2007), the use of PET methodologies in characterizing the function of the brain at rest is important, as the quantitative nature and physiological underpinnings of the method allows one to uncouple effects of blood flow, oxygen consumption, and glucose metabolism in the measured signal. Although technical considerations have led to the current situation where BOLD-fMRI is the more common method for visualizing the spatiotemporal dynamics of neural function, FDG-PET is a more direct and less confounded method for visualizing neuronal activity. The second benefit of fPET is that the method provides information about the dynamic use of the primary energy source of the brain—glucose. Univariate snapshots of glucose hypometabolism are predictive of neurodegeneration (e.g., Jack et al. 2013); however, preliminary evidence suggests that changes in the dynamic use of glucose over time may be an earlier and more powerful predictor of metabolic changes in neurodegenerative disease (Sanabria-Diaz et al. 2013). FDG-fPET methodology, therefore, represents an important development in characterizing metabolic connectivity in the human brain and may show promise as a biomarker for disease in the future.

Metabolic Covariance Is a Poor Predictor of Metabolic Connectivity

FDG-sPET metabolic covariance was dominated by left–right homologue, frontoparietal, temporosubcortical, and occipitotemporal covariance. This pattern is consistent with the earliest evidence of region-to-region correlation of the cerebral metabolic rate of glucose consumption (CMR_{GLC}) reported by Horwitz and colleagues over 30 years ago (e.g., Horwitz et al. 1984; Azari et al. 1994). In their early work, Horwitz and coleagues noted the paucity of positive correlations between the occipitotemporal and frontoparietal lobes; a finding that is evident in the present results where frontotemporal and parieto-occipital edges demonstrated negative correlations. Our sPET metabolic covariance results are also consistent with more recent published findings. Using a sPET acquisition, Di and Biswal (2012) reported that independent component analysis (ICA) decomposition revealed resting-state networks predominantly between left–right homotopic regions, with few networks showing anterior–posterior connectivity. In their follow-up report, Di et al. (2017) again found that sPET covariance is dominated by left–right homotopic connections and short-range connections within anatomical subdivisions, with only a few frontoparietal connections. Similarly, Savio et al. (2017) reported that sPET resting-state networks showed modest overlap with BOLD-fMRI networks but were sparser and less well-separated from each other compared with BOLD networks (see also Passow et al. 2015). In summary, the FDG-sPET metabolic covariance results in the present study are consistent with the extensive literature of previous resting-state studies.

We compared fPET connectivity to sPET covariance, since across-subject sPET covariance has (until the present study) been the established method for examining metabolic "connectivity" in health and disease (Yakushev et al. 2017). On the basis of previous comparisons of across- versus within-subject hemodynamic connectivity (Roberts et al. 2016), we hypothesized that sPET covariance would be moderately associated with fPET connectivity. Strikingly, we found that the sPET covariance matrix shows a high degree of unexplained variance when fPET connectivity was added to the model as a predictor. In other words, across-subject sPET covariance is a poor predictor of within-subject fPET connectivity. It is striking that the highest levels of unexplained variance was obtained in temporal and subcortical intrahemisphere (left–left and right–right) and interhemisphere (left–right, right–left) connections. This suggests that the left–right homologue covariance identified previously (e.g., Di and Biswal 2012; Di et al. 2017) may be an artifact of the across-subject correlation and poorly reflective of within-subject connectivity. This somewhat surprising finding is analogous to Simpson's Paradox (Simpson 1951) whereby a statistical relationship observed at a population level is reversed at the level of the individuals that constitute the population (Kievit et al. 2013). Conceptually, Simpson's Paradox refers to a sign reversal in the statistical relationships obtained at the individual and population (or group) levels. Roberts et al. (2016) found evidence of Simpson's Paradox for a number of brain regions in fMRI hemodynamic connectivity in the dorsal attention and default mode networks. However, they found that the majority of brain regions did not show a full reversal of the correlation values, as most brain regions showed across-subject correlations in the same direction as the within-subject correlations. Roberts and colleagues therefore concluded that across-subject

fMRI covariance is a reasonable predictor of within-subject fMRI connectivity.

While we did not directly test for Simpson's Paradox in our data, we found that there is a substantial amount of variability in the group-level sPET covariance matrix that was not explained by within-subject fPET connectivity. Simpson's Paradox is a special case of the "ecological fallacy" (Robinson 1950) and the related concept of "ergodicity" (Molenaar 2008; Kievit et al. 2013). Ergodic processes occur when a group-level result is generalizable to the individuals within the sample. In reality, ergodic processes are quite rare, because 2 strict criteria must be met: namely, the process must be homogeneous across individuals within a sample, and the statistical parameters that describe the process must be constant or stationary over time. Functional brain connectivity measured using neuroimaging data does not meet the criteria for ergodicity, and thus, group-level results are not generalizable to the individuals within the group (Fisher et al. 2018). Liégeois et al. (2017) have provided a complete mathematical examination of ergodicity in the context of BOLD-fMRI functional connectivity data. Due to technical limitations of the PET imaging method, existing studies of resting-state metabolic connectivity has been limited to examinations of group-level covariance rather than within-subject correlation of FDG-PET timeseries (e.g., Horwitz et al. 1984; Di et al. 2017; Savio et al. 2017). Researchers have attempted to draw quite strong conclusions on the basis of these results including attempts to use metabolic covariance as a biomarker for disease (Yakushev et al. 2017). A biomarker must, by definition, be estimable at the individual level (FDA-NIH 2019). Our results suggest that metabolic covariance cannot be used to predict within-subject connectivity. While sPET covariance analyses may be useful in other contexts, future attempts to explore metabolic connectivity as a biomarker for disease must necessarily use fPET as the only statistically valid approach.

FDG-fPET Metabolic Connectivity Is Correlated With BOLD-fMRI Hemodynamic Connectivity in Frontoparietal Regions

After controlling for FDG-fPET metabolic connectivity, the BOLD-fMRI connectivity matrix was uniformly slightly positive, with little variation across regions. In other words, fPET and fMRI share a greater amount of variance by comparison to fPET and sPET. The similarity between fPET and fMRI was also apparent when qualitatively comparing the network graphs and the distribution of the regions with higher degrees of connectivity. These results complement the recent findings of (Amend et al. 2019) who reported that FDG-fPET metabolic connectivity showed similarities to BOLD-fMRI hemodynamic connectivity in a rodent model. Our findings are also consistent with recent results of (Shokri-Kojori et al. 2019) who found that frontoparietal regions had the highest concurrent energy use (based on CMR_{GLC}) and BOLD-fMRI activity, in comparison to the rest of the brain.

One puzzling finding was the low degree apparent in subcortical regions for both FDG-fPET and BOLD-fMRI. Indeed, this effect was also apparent for the FDG-sPET results. These observations are in contrast with the known high degree of interconnectedness of the subcortical regions with the rest of the brain: the corticobasal ganglia–cerebellar (Middleton and Strick 2000; Bostan and Strick 2010) and corticothalamic circuits (Parent and Hazrati 1995). These results are likely attributable to the reduced sensitivity of signal detection in midbrain areas for both PET and fMRI (Supplementary Fig. S3). Smaller subcortical structures are also likely to be subject to partial volume effects (Hoffman et al. 1979), particularly in PET data that have a physical limit in spatial resolution due to the positron range (Moses 2011), which may also contribute to this result. Reconstruction techniques to improve PET spatial resolution and postprocessing techniques to reduce partial volume effects (Sudarshan et al. 2020) may result in higher quality and greater brain coverage of the fPET connectivity matrices.

Direct comparisons between FDG-fPET and BOLD-fMRI are in part limited by the differences in temporal resolution and SNR of the 2 imaging modalities. The FDG-fPET protocol involves the administration of low levels of radioactivity over an extended time period, and results in PET images with lower signal and greater noise in comparison to BOLD-fMRI. Neural activity is optimally investigated using imaging techniques that have temporal resolutions in the order of milliseconds, which cannot be achieved by either fPET or fMRI. Nevertheless, the temporal resolution of conventional fMRI has been enormously useful for characterizing distributed brain activity involving networks with multiple synapses over large-scale pathways in the brain. Importantly, although our understanding of integrative human brain networks has been developed largely from fMRI experimental results, the technique cannot serve as a "ground-truth" for brain networks that are identifiable using FDG-fPET. In addition to the inherent methodological limitations of fMRI, the FDG-fPET and BOLD-fMRI experimental techniques detect different physiological targets, namely neural glucose metabolism and deoxygenation of hemoglobin in the cerebrovasculature. In comparison to the large body of literature of fMRI networks and brain connectivity, the evaluation of fPET resting-state networks is based on FDG-PET as a direct and quantitative index of neural metabolic activity without cerebrovascular confounds (Magistretti et al. 1999). Multimodality imaging including simultaneous MR-PET has motivated important developments in PET detector technology, which have led to improved sensitivity for low-signal detection methods including fPET (Chen et al. 2018). Future PET detector technologies may have the potential to further improve the detection sensitivity, which have the potential for the temporal resolution of fPET to approach that of fMRI.

Future Directions

A limitation of the FDG-fPET methodology is that the biosafety constraints on the dose of the administered radioactivity produce noisy PET images with low SNR. The differing SNR profiles between the sPET, fPET, and fMRI modalities motivated the use of a percentile "thresholding" approach, rather than a statistical threshold, which would likely require different thresholds for each modality due to differences in statistical power. The percentile approach allowed comparison of the most highly connected regions between the modalities. We note that the atlas-based decomposition (ROI) analysis of resting-state connectivity that we applied is less sensitive to the signal-to-noise limitations of fPET, and thus, higher signal-to-noise timeseries data would likely be required for individual voxel-based analyses. The potential of the FDG-fPET technique is that it theoretically provides a more direct measure of neuronal activity than fMRI and does not have the susceptibility artifacts present in BOLD-fMRI. However, this advantage may not be realized in practice as the connectivity estimates in subcortical regions, which are some of the most interconnected regions in the human brain, showed low-region degree in both FDG-fPET and BOLD-fMRI.

This limitation may be addressed through postprocessing techniques that can improve PET resolution by using synergistic MR-PET reconstruction techniques (Sudarshan et al. 2020). Future work should aim to further characterize and improve the noise properties of the fPET signal, as well as optimize the acquisition and data preparation procedures.

We encountered a technical limitation during PET postprocessing that future work should address. The reconstruction software was unable to provide noninteger second fPET bins, which prevented reconstruction of the PET listmode data into images that had a time duration that was a multiple of the fMRI TR. One consequence is that a phase shift may result in the temporal synchrony of the fMRI and fPET timeseries data. Future work should consider this potential limitation at the experiment–design phase. Reconstruction of fPET frames into a multiple of the fMRI TR would also facilitate examination of temporal similarity between the two signals. An additional technical limitation is that the processing pipeline for FDG-fPET data is immature in comparison to the preprocessing procedures for BOLD-fMRI data. As a nascent technology, FDG-fPET has not had the benefit of many years of work validating acquisition parameters, data preparation, and signal detection optimization, including characterizing of potential physiological artifacts that may be possible to remove with filtering techniques. Work in these fields are presently improving the radiotracer administration (e.g., Jamadar et al. 2019a; Rischka et al. 2018), attenuation correction (Baran et al. 2018), motion correction (Chen et al. 2019), and data analysis (Li et al. 2019) techniques.

An important distinction to make is that the brain connectivity reported here is not comparable to "dynamic" connectivity as reported in the literature over the past few years. While the fPET metabolic connectivity measures are dynamic in the sense that they cross-correlate the regional "time-courses" of FDG uptake over the scan period, the approach is nevertheless temporally invariant (stationary) as the correlation is expected to be robust to temporal reordering of the measurement time-points. In other words, the Pearson r values describing the metabolic connectivity would be unchanged by permuting the order of the PET images. While other authors have used the term "static" to refer to stationary measures of functional connectivity, we do not use the term "static metabolic connectivity" to avoid confusion with our use of sPET to denote across-subject PET covariance (see Liégeois et al. 2017 for discussion of static vs. dynamic functional connectivity and the mathematical basis of stationarity in hemodynamic connectivity). Our approach to analyze stationary fPET metabolic connectivity was to compare metabolic connectivity with the most common method for estimation of functional connectivity in the BOLD-fMRI literature (Liégeois et al. 2017; Preti et al. 2017), which is the basis of our knowledge of integrative brain connectivity. However, truly "dynamic" brain connectivity does take into account the temporal fluctuations of functional and metabolic connectivity, since the temporal ordering of the timeseries of brain images is important (Calhoun et al. 2014). Dynamic connectivity approaches include sliding-time window approaches and models of switching between microstates (Preti et al. 2017). While it is important that future studies examine the dynamics of FDG-fPET metabolic connectivity, the current temporal resolution of fPET methodology will present a major challenge.

Conclusion

Simultaneous neuroimaging studies that independently measure brain function are by nature challenging. Data from each imaging modality are optimally acquired using a distinctive experimental protocol and instrumentation that may adversely influence the integrity of the complementary measures of brain function. Simultaneous FDG-PET/BOLD-fMRI represents a significant advance over previous approaches. Our experimental approach to simultaneously image two mechanisms that underpin the dynamics of energy consumption in the brain via glucose metabolism and the cerebrovascular hemodynamic response provides a unique opportunity to investigate the fundamental basis of human brain connectivity. In this study, we have reported the first FDG-fPET metabolic connectivity in humans and discovered that metabolic connectivity is more predictive of BOLD-fMRI hemodynamic connectivity than conventional FDG-PET metabolic covariance measures. Notably, these findings motivate and provide a basis for future metabolic brain connectivity studies across the human life span and investigations of novel biomarkers for neurological and neurodegenerative diseases.

Supplementary Material

Supplementary material can be found at *Cerebral Cortex* online.

Authors Contributions

S.D.J., P.G.D.W., and G.F.E. designed the research question; P.G.D.W., E.X.L., and E.R.O. conducted the analysis, S.D.J. wrote the first draft of the paper with G.F.E. and P.G.D.W. edits. All authors contributed to manuscript preparation and review. G.F.E., S.D.J., and Z.C. sourced funding for the work.

Notes

The authors acknowledge Richard McIntyre, Alexandra Carey, Disha Sasan, and Irene Graafsma from Monash Biomedical Imaging for their assistance in acquiring data. *Conflict of interest*: None declared.

Data Availability

Data are available at OpenNeuro with the accession number ds002898; https://openneuro.org/datasets/ds002898/versions/1.1.0.

Funding

Australian Research Council (ARC) Linkage Project with Siemens Healthineers (LP170100494); ARC Centre of Excellence for Integrative Brain Function (CE140100007 to G.F.E., S.D.J., and P.G.D.W.); ARC Discovery Early Career Researcher Award (DE150100406 to S.D.J.); National Health and Medical Research Council Fellowship (APP1174164 to S.D.J.).

References

Alderson TH, Bokde ALW, Kelso JAS, Maguire L, Coyle D. 2020. Metastable neural dynamics underlies cognitive performance across multiple behavioural paradigms. *Hum Brain Mapp*. hbm.25009. doi: 10.1002/hbm.25009.

Amend M, Ionescu TM, Di X, Pichler BJ, Biswal BB, Wehrl HF. 2019. Functional resting-state brain connectivity is accompanied by dynamic correlations of application-dependent [18F]FDG PET-tracer fluctuations. *Neuroimage*. 196:161–172. doi: 10.1016/j.neuroimage.2019.04.034.

Andrews-Hanna JR, Snyder AZ, Vincent JL, Lustig C, Head D, Raichle ME, Buckner RL. 2007. Disruption of large-scale brain systems in advanced aging. *Neuron*. 56:924–935. doi: 10.1016/j.neuron.2007.10.038.

Avants BB, Tustison NJ, Song G, Cook PA, Klein A, Gee JC. 2011. A reproducible evaluation of ANTs similarity metric performance in brain image registration. *Neuroimage*. 54:2033–2044. doi: 10.1016/j.neuroimage.2010.09.025.

Azari NP, Horwitz B, Pettigrew KD, Grady CL, Haxby JV, Giacometti KR, Schapiro MB. 1994. Abnormal pattern of cerebral glucose metabolic rates involving language areas in young adults with down syndrome. *Brain Lang*. 46:1–20. doi: 10.1006/brln.1994.1001.

Baran J, Chen Z, Sforazzini F, Ferris N, Jamadar S, Schmitt B, Faul D, Shah NJ, Cholewa M, Egan GF. 2018. Accurate hybrid template–based and MR-based attenuation correction using UTE images for simultaneous PET/MR brain imaging applications. *BMC Med Imaging*. 18:41. doi: 10.1186/s12880-018-0283-3.

Biswal B, Yetkin FZ, Haughton VM, Hyde JS. 1995. Functional connectivity in the motor cortex of resting human brain using echo-planar MRI. *Magn Reson Med*. 34:537–541. doi: 10.1002/mrm.1910340409.

Bostan AC, Strick PL. 2010. The cerebellum and basal ganglia are interconnected. *Neuropsychol Rev*. 20:261–270. doi: 10.1007/s11065-010-9143-9.

Burgos N, Cardoso MJ, Thielemans K, Modat M, Pedemonte S, Dickson J, Barnes A, Ahmed R, Mahoney CJ, Schott JM et al. 2014. Attenuation correction synthesis for hybrid PET-MR scanners: application to brain studies. *IEEE Trans Med Imaging*. 33:2332–2341. doi: 10.1109/TMI.2014.2340135.

Calhoun VD, Miller R, Pearlson G, Adalı T. 2014. The Chronnectome: time-varying connectivity networks as the next frontier in fMRI data discovery. *Neuron*. 84:262–274. doi: 10.1016/j.neuron.2014.10.015.

Chen Z, Jamadar SD, Li S, Sforazzini F, Baran J, Ferris N, Shah NJ, Egan GF. 2018. From simultaneous to synergistic MR-PET brain imaging: a review of hybrid MR-PET imaging methodologies. *Hum Brain Mapp*. 39:5126–5144. doi: 10.1002/hbm.24314.

Chen Z, Sforazzini F, Baran J, Close T, Shah NJ, Egan GF. 2019. MR-PET head motion correction based on co-registration of multicontrast MR images. *Hum Brain Mapp*. doi: 10.1002/hbm.24497.

Cox RW. 1996. AFNI: software for analysis and visualization of functional magnetic resonance Neuroimages. *Comput Biomed Res*. 29:162–173. doi: 10.1006/cbmr.1996.0014.

Di X, Biswal B. 2012. Metabolic brain covariant networks as revealed by FDG-PET with reference to resting-state fMRI networks. *Brain Connect*. 2:275–283. doi: 10.1089/brain.2012.0086.

Di X, Gohel S, Thielcke A, Wehrl HF, Biswal BB, The Alzheimer's Disease Neuroimaging Initiative. 2017. Do all roads lead to Rome? A comparison of brain networks derived from inter-subject volumetric and metabolic covariance and moment-to-moment hemodynamic correlations in old individuals. *Brain Struct Funct*. 222:3833–3845. doi: 10.1007/s00429-017-1438-7.

Diedrichsen J, Balsters JH, Flavell J, Cussans E, Ramnani N. 2009. A probabilistic MR atlas of the human cerebellum. *Neuroimage*. 46(1):39–46.

Dixon ML, De La Vega A, Mills C, Andrews-Hanna J, Spreng RN, Cole MW, Christoff K. 2008. Heterogeneity within the frontoparietal control network and its relationship to the default and dorsal attention networks. *Proc Natl Acad Sci U S A*. 115(7):E1598–E1607.

Fisher AJ, Medaglia JD, Jeronimus BF. 2018. Lack of group-to-individual generalizability is a threat to human subjects research. *Proc Natl Acad Sci U S A*. 115:E6106–E6115. doi: 10.1073/pnas.1711978115.

FDA-NIH Biomarker Working Group. 2019 BEST (Biomarkers, EndpointS, and other Tools) Resource [Internet]. Silver Spring (MD): Food and Drug Administration (US). Available from: https://www.ncbi.nlm.nih.gov/books/NBK326791/. Co-published by National Institutes of Health (US), Bethesda (MD).

Fornito A, Bullmore ET. 2010. What can spontaneous fluctuations of the blood oxygenation-level-dependent signal tell us about psychiatric disorders? *Curr Opin Psychiatry*. 23:239–249. doi: 10.1097/YCO.0b013e328337d78d.

Fox MD, Raichle ME. 2007. Spontaneous fluctuations in brain activity observed with functional magnetic resonance imaging. *Nat Rev Neurosci*. 8:700–711. doi: 10.1038/nrn2201.

Fox MD, Snyder AZ, Vincent JL, Raichle ME. 2007. Intrinsic fluctuations within cortical systems account for intertrial variability in human behavior. *Neuron*. 56:171–184. doi: 10.1016/j.neuron.2007.08.023.

Hahn A, Breakspear M, Rischka L, Wadsak W, Godbersen GM, Pichler V, Michenthaler P, Vanicek T, Hacker M, Kasper S et al. 2020. Reconfiguration of functional brain networks and metabolic cost converge during task performance. *eLife*. 9:e52443. doi: 10.7554/eLife.52443.

Hahn A, Gryglewski G, Nics L, Hienert M, Rischka L, Vraka C, Sigurdardottir H, Vanicek T, James GM, Seiger R et al. 2016. Quantification of task-specific glucose metabolism with constant infusion of 18F-FDG. *J Nucl Med*. 57:1933–1940. doi: 10.2967/jnumed.116.176156.

Hahn A, Gryglewski G, Nics L, Rischka L, Ganger S, Sigurdardottir H, Vraka C, Silberbauer L, Vanicek T, Kautzky A et al. 2017. Task-relevant brain networks identified with simultaneous PET/MR imaging of metabolism and connectivity. *Brain Struct Funct*. 1–10. doi: 10.1007/s00429-017-1558-0.

Hoffman EJ, Huang S-C, Phelps ME. 1979. Quantitation in positron emission computed tomography: 1. Effect of object size. *J Comput Assist Tomogr*. 3:299–308. doi:10.1097/00004728-197906000-00001.

Hohenfeld C, Werner CJ, Reetz K. 2018. Resting-state connectivity in neurodegenerative disorders: is there potential for an imaging biomarker? *NeuroImage: Clin*. 18:849–870. doi: 10.1016/j.nicl.2018.03.013.

Horwitz B, Duara R, Rapoport SI. 1984. Intercorrelations of glucose metabolic rates between brain regions: application to healthy males in a state of reduced sensory input. *J Cereb Blood Flow Metab*. 4:484–499. doi: 10.1038/jcbfm.1984.73.

Jack CR, Knopman DS, Jagust WJ, Petersen RC, Weiner MW, Aisen PS, Shaw LM, Vemuri P, Wiste HJ, Weigand SD et al. 2013. Tracking pathophysiological processes in Alzheimer's disease: an updated hypothetical model of dynamic biomarkers. *The Lancet Neurology*. 12:207–216. doi: 10.1016/S1474-4422(12)70291-0.

Jamadar SD, Egan GF, Calhoun VD, Johnson B, Fielding J. 2016. Intrinsic connectivity provides the baseline framework for variability in motor performance: a multivariate fusion analysis of low- and high-frequency resting-state oscillations and antisaccade performance. *Brain Connect*. 6:505–517. doi: 10.1089/brain.2015.0411.

Jamadar SD, Sforazzini F, Raniga P, Ferris NJ, Paton B, Bailey MJ, Brodtmann A, Yates PA, Donnan GA, Ward SA et al. 2018. Sexual dimorphism of resting-state network connectivity in healthy ageing. *J Gerontol B Psychol Sci Soc Sci*. doi: 10.1093/geronb/gby004.

Jamadar SD, Ward PGD, Carey A, McIntyre R, Parkes L, Sasan D, Fallon J, Orchard E, Li S, Chen Z et al. 2019a. Radiotracer administration for high temporal resolution positron emission tomography of the human brain: application to FDG-fPET. *JoVE*. 60259. doi: 10.3791/60259.

Jamadar SD, Ward PGD, Li S, Sforazzini F, Baran J, Chen Z, Egan GF. 2019b. Simultaneous task-based BOLD-fMRI and [18-F] FDG functional PET for measurement of neuronal metabolism in the human visual cortex. *Neuroimage*. 189:258–266. doi: 10.1016/j.neuroimage.2019.01.003.

Jamadar SD, Ward PGD, Close TG, Fornito A, Premaratne M, O'Brien K, Stäb D, Chen Z, Shah NJ, Egan GF. 2020. Simultaneous BOLD-fMRI and constant infusion FDG-PET data of the resting human brain. *Scientific Data*. 7:Article number 363.

Jenkinson M, Bannister P, Brady M, Smith S. 2002. Improved optimization for the robust and accurate linear registration and motion correction of brain images. *Neuroimage*. 17:825–841. doi: 10.1006/nimg.2002.1132.

Jenkinson M, Beckmann CF, Behrens TEJ, Woolrich MW, Smith SM. 2012. FSL 20 years of fMRI20 years of fMRI. *Neuroimage*. 62:782–790. doi: 10.1016/j.neuroimage.2011.09.015.

Judenhofer MS, Wehrl HF, Newport DF, Catana C, Siegel SB, Becker M, Thielscher A, Kneilling M, Lichy MP, Eichner M et al. 2008. Simultaneous PET-MRI: a new approach for functional and morphological imaging. *Nat Med*. 14:459–465. doi: 10.1038/nm1700.

Kievit RA, Frankenhuis WE, Waldorp LJ, Borsboom D. 2013. Simpson's paradox in psychological science: a practical guide. *Front Psychol*. 4. doi: 10.3389/fpsyg.2013.00513.

Laird AR, Fox PM, Eickhoff SB, Turner JA, Ray KL, McKay DR, Glahn DC, Beckmann CF, Smith SM, Fox PT. 2011. Behavioral interpretations of intrinsic connectivity networks. *J Cogn Neurosci*. 23:4022–4037. doi: 10.1162/jocn_a_00077.

Li S, Jamadar SD, Ward PGD, Premaratne M, Egan GF, Chen Z. 2019. Analysis of continuous infusion functional PET (fPET) in the human brain (preprint). *Neuroscience*. doi: 10.1101/778357.

Liégeois R, Laumann TO, Snyder AZ, Zhou J, Yeo BTT. 2017. Interpreting temporal fluctuations in resting-state functional connectivity MRI. *Neuroimage*. 163:437–455. doi: 10.1016/j.neuroimage.2017.09.012.

Liu TT. 2017. Reprint of 'noise contributions to the fMRI signal: an overview'. *NeuroImage, Cleaning up the fMRI time series: mitigating noise with advanced acquisition and correction strategies*. 154:4–14. doi: 10.1016/j.neuroimage.2017.05.031.

Logothetis NK. 2008. What we can do and what we cannot do with fMRI. *Nature*. 453:869–878. doi: 10.1038/nature06976.

Magistretti, PJ, Pellerin, L. 1999. Cellular mechanisms of brain energy metabolism and their relevance to functional brain imaging. *Philos Trans R Soc Lond B Biol Sci*. 354:1155–1163.

Magistretti PJ, Allaman I. 2015. A cellular perspective on brain energy metabolism and functional imaging. *Neuron*. 86:883–901. doi: 10.1016/j.neuron.2015.03.035.

Middleton F, Strick P. 2000. Basal ganglia and cerebellar loops: motor and cognitive circuits. *Brain Res Rev*. 31:236–250. doi: 10.1016/S0165-0173(99)00040-5.

Moeller JR, Strother SC, Sidtis JJ, Rottenberg DA. 1987. Scaled subprofile model: a statistical approach to the analysis of functional patterns in positron emission tomographic data. *J Cereb Blood Flow Metab*. 7:649–658. doi: 10.1038/jcbfm.1987.118.

Molenaar PCM. 2008. On the implications of the classical ergodic theorems: analysis of developmental processes has to focus on intra-individual variation. *Dev Psychobiol*. 50:60–69. doi: 10.1002/dev.20262.

Moses WW. 2011. Fundamental limits of spatial resolution in PET. *Nucl Instrum Methods Phys Res, Sect A*. 648:S236–S240. doi: 10.1016/j.nima.2010.11.092.

Murphy K, Fox MD. 2017. Towards a consensus regarding global signal regression for resting state functional connectivity MRI. *Neuroimage*. 154:169–173. doi: 10.1016/j.neuroimage.2016.11.052.

Ogawa S, Lee T, Kay A, Tank D. 1990. Brain magnetic resonance imaging with contrast dependent on blood oxygenation. *Proc Natl Acad Sci*. 87:9868–9872.

Parent A, Hazrati L-N. 1995. Functional anatomy of the basal ganglia. I. The cortico-basal ganglia-thalamo-cortical loop. *Brain Res Rev*. 20:91–127. doi: 10.1016/0165-0173(94)00007-C.

Passow S, Specht K, Adamsen TC, Biermann M, Brekke N, Craven AR, Ersland L, Grüner R, Kleven-Madsen N, Kvernenes O-H et al. 2015. Default-mode network functional connectivity is closely related to metabolic activity: metabolic activity and DMN connectivity. *Hum Brain Mapp*. 36:20272038. doi: 10.1002/hbm.22753.

Phillips AA, Chan FH, Zheng MMZ, Krassioukov AV, Ainslie PN. 2016. Neurovascular coupling in humans: physiology, methodological advances and clinical implications. *J Cereb Blood Flow Metab*. 36:647–664. doi: 10.1177/0271678X15617954.

Preti MG, Bolton TA, Van De Ville D. 2017. The dynamic functional connectome: state-of-the-art and perspectives. *Neuroimage*. 160:41–54. doi: 10.1016/j.neuroimage.2016.12.061.

Raichle ME, MacLeod AM, Snyder AZ, Powers WJ, Gusnard DA, Shulman GL. 2001. A default mode of brain function. *Proc Natl Acad Sci*. 98:676–682. doi: 10.1073/pnas.98.2.676.

Raichle ME, Snyder AZ. 2007. A default mode of brain function: a brief history of an evolving idea. *Neuroimage*. 37:1083–1090. doi: 10.1016/j.neuroimage.2007.02.041.

Rischka L, Gryglewski G, Pfaff S, Vanicek T, Hienert M, Klöbl M, Hartenbach M, Haug A, Wadsak W, Mitterhauser M et al. 2018. Reduced task durations in functional PET imaging with [18F]FDG approaching that of functional MRI. *Neuroimage*. 181:323–330. doi: 10.1016/j.neuroimage.2018.06.079.

Roberts RP, Hach S, Tippett LJ, Addis DR. 2016. The Simpson's paradox and fMRI: similarities and differences between functional connectivity measures derived from within-subject and across-subject correlations. *Neuroimage*. 135:1–15. doi: 10.1016/j.neuroimage.2016.04.028.

Robinson WS. 1950. Ecological correlations and the behavior of individuals. *Int J Epidemiol*. 38:337–341.

Sanabria-Diaz G, Martínez-Montes E, Melie-Garcia L, the Alzheimer's Disease Neuroimaging Initiative. 2013. Glucose metabolism during resting state reveals abnormal brain networks organization in the Alzheimer's disease and mild cognitive impairment. *PLoS One*. 8:e68860. doi: 10.1371/journal.pone.0068860.

Sasaki H, Kanno I, Murakami M, Shishido F, Uemura K. 1986. Tomographic mapping of kinetic rate constants in the fluorodeoxyglucose model using dynamic positron emission tomography. *J Cereb Blood Flow Metab*. 6:447–454. doi: 10.1038/jcbfm.1986.78.

Savio A, Fünger S, Tahmasian M, Rachakonda S, Manoliu A, Sorg C, Grimmer T, Calhoun V, Drzezga A, Riedl V et al.

2017. Resting-state networks as simultaneously measured with functional MRI and PET. *J Nucl Med*. 58:1314–1317. doi: 10.2967/jnumed.116.185835.

Shokri-Kojori E, Tomasi D, Alipanahi B, Wiers CE, Wang G-J, Volkow ND. 2019. Correspondence between cerebral glucose metabolism and BOLD reveals relative power and cost in human brain. *Nat Commun*. 10:690. doi: 10.1038/s41467-019-08546-x.

Shulman GL, Fiez JA, Corbetta M, Buckner RL, Miezin FM, Raichle ME, Petersen SE. 1997. Common blood flow changes across visual tasks: II. Decreases in cerebral cortex. *J Cogn Neurosci*. 9:648–663. doi: 10.1162/jocn.1997.9.5.648.

Simpson EH. 1951. The interpretation of interaction in contingency tables. *J R Stat Soc B Methodol*. 13:238–241.

Smith SM. 2002. Fast robust automated brain extraction. *Hum Brain Mapp*. 17:143–155. doi: 10.1002/hbm.10062.

Sokoloff L. 1981. The deoxyglucose method for the measurement of local glucose utilization and the mapping of local functional activity in the central nervous system. In: *International Review of Neurobiology*. Academic Press: New York, pp. 287–333. doi: 10.1016/S0074-7742(08)60296-2

Sokoloff L, Reivich M, Kennedy C, Rosiers MHD, Patlak CS, Pettigrew KD, Sakurada O, Shinohara M. 1977. The [14C]Deoxyglucose method for the measurement of local cerebral glucose utilization: theory, procedure, and normal values in the conscious and anesthetized albino rat. *J Neurochem*. 28:897–916. doi: 10.1111/j.1471-4159.1977.tb10649.x.

Sudarshan VP, Li S, Jamadar SD, Egan GF, Awate SP, Chen Z. 2020. Improved temporal resolution for mapping brain metabolism using functional PET and anatomical MRI knowledge (preprint). *Neuroscience*. doi: 10.1101/2020.07.08.192872.

Ter-Pogossian MM. 1992. The origins of positron emission tomography. *Semin Nucl Med*. 22:140–149. doi: 10.1016/S0001-2998(05)80142-4.

Tustison NJ, Avants BB, Cook PA, Zheng Y, Egan A, Yushkevich PA, Gee JC. 2010. N4ITK: improved N3 bias correction. *IEEE Trans Med Imaging*. 29:1310–1320. doi: 10.1109/TMI.2010.2046908.

Vaishnavi SN, Vlassenko AG, Rundle MM, Snyder AZ, Mintun MA, Raichle ME. 2010. Regional aerobic glycolysis in the human brain. *PNAS*. 107:17757–17762. doi: 10.1073/pnas.1010459107.

Veronese M, Moro L, Arcolin M, Dipasquale O, Rizzo G, Expert P, Khan W, Fisher PM, Svarer C, Bertoldo A et al. 2019. Covariance statistics and network analysis of brain PET imaging studies. *Sci Rep*. 9:2496. doi: 10.1038/s41598-019-39005-8.

Villien M, Wey H-Y, Mandeville JB, Catana C, Polimeni JR, Sander CY, Zürcher NR, Chonde DB, Fowler JS, Rosen BR et al. 2014. Dynamic functional imaging of brain glucose utilization using fPET-FDG. *Neuroimage*. 100:192–199. doi: 10.1016/j.neuroimage.2014.06.025.

Ward PGD, Orchard ER, Oldham S, Arnatkevičiūtė A, Sforazzini F, Fornito A, Egan GF, Jamadar SD. 2019. Individual differences in haemoglobin concentration influence BOLD fMRI functional connectivity and its correlation with cognition (preprint). *Neuroscience*. doi: 10.1101/835660.

Yakushev I, Drzezga A, Habeck C. 2017. Metabolic connectivity. *Curr Opin Neurol*. 30:677–685. doi: 10.1097/WCO.0000000000000494.

Yeo BT, Krienen FM, Sepulcre J, Sabuncu MR, Lashkari D, Hollinshead M, Roffman JL, Smoller JW, Zöllei L, Polimeni JR et al. 2011. The organization of the human cerebral cortex estimated by intrinsic functional connectivity. *J Neurophysiol*. 106:1125–1165. doi: 10.1152/jn.00338.2011.